Reaction zone structure for strong, weak overdriven, and weak underdriven oblique detonations

Joseph M. Powers[a] and Keith A. Gonthier[b]
Department of Aerospace and Mechanical Engineering, University of Notre Dame, Notre Dame, Indiana 46556-5637

(Received 5 February 1992; accepted 26 May 1992)

A simple dynamic systems analysis is used to give examples of strong, weak overdriven, and weak underdriven oblique detonations. Steady oblique detonations consisting of a straight lead shock attached to a solid wedge followed by a resolved reaction zone structure are admitted as solutions to the reactive Euler equations. This is demonstrated for a fluid that is taken to be an inviscid, calorically perfect ideal gas that undergoes a two-step irreversible reaction with the first step exothermic and the second step endothermic. This model admits solutions for a continuum of shock wave angles for two classes of solutions identified by a Rankine–Hugoniot analysis: strong and weak overdriven waves. The other class, weak underdriven, is admitted for eigenvalue shock-wave angles. Chapman–Jouguet waves, however, are not admitted. These results contrast those for a corresponding one-step model that, for detonations with a straight lead shock, only admits strong, weak overdriven, and Chapman–Jouguet solutions.

I. INTRODUCTION

Revived interest in hypersonic flight has generated interest in devices that employ oblique detonations. An oblique detonation is defined as a combustion process that is induced by an oblique shock. Most recent discussion of oblique detonations has been motivated by the oblique detonation wave engine (ODWE), which has been proposed to propel the National Aerospace Plane (NASP), and the ram accelerator, which has been used to accelerate projectiles to high speeds.

Figure 1 gives a diagram of the type of oblique detonation to be studied here along with the coordinate system. We consider an incoming unreacted gaseous mixture at supersonic Mach number $M_0 > 1$, which encounters a straight shock, inclined at angle β to the horizontal, which is attached to a curved wedge. The mixture reacts downstream of the shock in the reaction zone. We consider the special case in which the flow has variation in the direction normal to the shock, taken to be the x direction, but no variation in the direction parallel to the shock, taken to be the y direction. The origin is taken to be the wedge tip. The streamlines are taken to form an angle θ with the horizontal. At complete reaction, θ relaxes to a constant value, which we call the wedge angle. The flow has symmetry about the horizontal plane.

Rankine–Hugoniot (RH) analysis has been commonly used to restrict the potential equilibrium states which may be obtained in an oblique detonation (Siestrunck *et al.*,[1] Larisch,[2] Gross and Chinitz,[3] Gross,[4] Oppenheim *et al.*,[5] Chernyi,[6] and Pratt *et al.*[7]). The RH analysis allows determination of both β, θ shock and detonation polars. For $M_0 = 10$ and specific heat ratio $\gamma = 7/5$, Fig. 2 shows such polars for an inert oblique shock, $Q = 0$, and a complete reaction oblique detonation, $Q = 25$, where Q is a dimensionless heat release to be defined later. Following Pratt *et al.*, we use the final value of the Mach number normal to the shock, M_x, and analogies with inert oblique shock nomenclature to classify oblique detonations. For shock angles below a critical value $\beta < \beta_{CJ}$, there is no real solution to the RH equations. For $\beta = \beta_{CJ}$, there is one solution that corresponds to the Chapman–Jouguet (CJ) solution of one-dimensional theory. For $\beta = \beta_{CJ}$, at complete reaction the normal Mach number is sonic, $M_x = 1$. For $\beta > \beta_{CJ}$, two solutions are obtained. The solution corresponding to the smaller wedge angle has a supersonic normal Mach number, $M_x > 1$, at complete reaction and is known as a weak underdriven solution. Its counterpart with the higher wedge angle is known as a weak overdriven solution if $\beta < \beta_{detach}$ and a strong solution if $\beta \geqslant \beta_{detach}$. For both weak overdriven and strong solutions, the final normal Mach number is subsonic, $M_x < 1$. Here, β_{detach} is the shock angle corresponding to the wedge angle θ_{detach} beyond which there is no attached shock solution. The nomenclature "weak" and "strong" is suggested by oblique shock theory and is not consistent with the nomenclature of one-dimensional detonation theory.

The two-dimensional steady flow can be further characterized by the hyperbolic or elliptic character of the governing partial differential equations. With the total Mach number M calculated from the velocity magnitude, the equations are elliptic if $M < 1$ and hyperbolic if $M > 1$. The subsonic to supersonic transition takes place at β_{SS} which is slightly less than β_{detach}. Strong solutions terminate at a subsonic point, $M < 1$. Weak overdriven solutions terminate at either subsonic or supersonic points: for $\beta_{CJ} < \beta < \beta_{SS}$, $M > 1$; for $\beta_{SS} < \beta < \beta_{detach}$, $M < 1$. Generally, $\beta_{SS} \sim \beta_{detach}$; consequently the range of weak overdriven solutions with $M < 1$ is small. Weak underdriven solutions terminate at supersonic points, $M > 1$.

The conditions under which these solution classes,

[a] Assistant professor. All correspondence should be sent to this author.
[b] Graduate assistant.

 0899-8213/92/092082-08$04.00

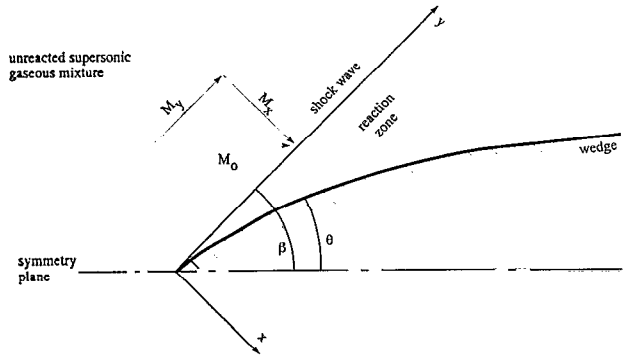

FIG. 1. Schematic of an oblique detonation with a straight shock attached to a curved wedge.

each of which satisfies the conservation principles and entropy inequality, could exist in nature is a question that has not been completely answered. A first step is to consider the resolved steady reaction zone structures and examine solution trajectories from an initial state to an equilibrium state in phase space. For a given kinetic scheme, this will disqualify certain classes of solutions. Those that remain should be subjected to the more rigorous test of hydrodynamic stability. What should result is a knowledge of the initial and boundary conditions that are necessary for a solution to exist. Based on analogies with inert theory that show that the existence of a strong or weak oblique shock depends on the downstream boundary conditions, it is hypothesized that there may be boundary conditions for each class of oblique detonation to exist. Given that, in the course of its travels, both an ODWE and ram accelerator may encounter boundary conditions suitable for each class of oblique detonation, it stands to reason that each class should be subjected to systematic study.

With this philosophy in mind, Powers and Stewart[8] have carried out a study of steady reaction zone structures associated with oblique detonations in which the reaction is one-step and irreversible. With such a kinetic model and for an oblique detonation that includes a straight lead shock, it was shown that the reactive Euler equations admit strong, weak overdriven, and CJ solutions but do not admit weak underdriven solutions.

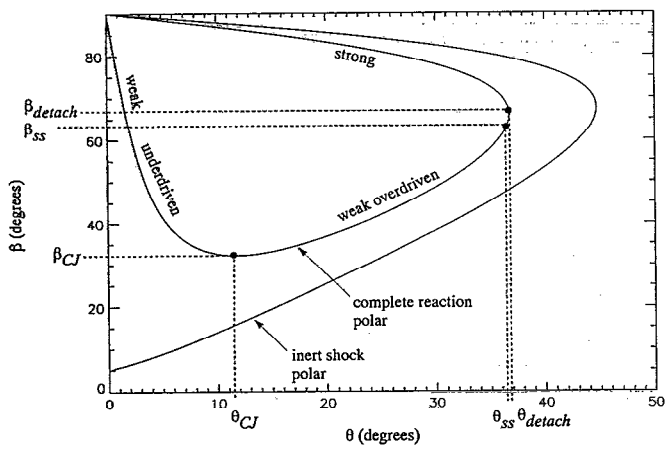

FIG. 2. Inert $[Q(0,0)=0]$ and complete reaction $[Q(1,1)=25]$ polars $(M_0=10,\gamma=7/5)$.

In the present study, we generalize the model of Ref. 8 to allow for a two-step irreversible reaction with the first step exothermic and the second endothermic. For completeness, we present examples for all three classes of oblique detonations. *However, our primary purpose is to demonstrate that weak underdriven oblique detonations are admissible solutions. To this end, a specifically designed and particularly simple geometry and model are employed.* The wedge geometry is chosen so as to guarantee an attached straight shock. The model has the same functional form as models that are commonly used to simulate the combustion of real materials; it is a two-dimensional extension of a model used by Fickett and Davis[9] (pp. 153–173) to predict one-dimensional weak or eigenvalue detonations. As suggested in Ref. 8, use of this model leads to a two-dimensional complement of the eigenvalue detonation.

The plan of this paper is as follows. First, the model equations are presented. These are reduced to a set of ordinary differential equations by assuming there are no changes in the direction tangent to the shock. Exact expressions are then written for strong and weak overdriven oblique detonations in the hypersonic limit. Away from the hypersonic limit, numerical integration of ordinary differential equations gives the reaction zone structure. Examples of strong, weak overdriven, and weak underdriven oblique detonations are presented. It is shown for this system that there is no trajectory in phase space to a complete reaction state for a CJ oblique detonation.

II. MODEL EQUATIONS

We adopt many of the assumptions and nomenclature of Fickett and Davis.[9] The model equations are taken to be the two-dimensional steady Euler and species evolution equations for a reactive calorically perfect ideal gas. These are expressed in dimensionless conservative form:

$$\frac{\partial}{\partial x}(\rho u)+\frac{\partial}{\partial y}(\rho v)=0, \tag{1}$$

$$\frac{\partial}{\partial x}(\rho u^2+P)+\frac{\partial}{\partial y}(\rho uv)=0, \tag{2}$$

$$\frac{\partial}{\partial x}(\rho uv)+\frac{\partial}{\partial y}(\rho v^2+P)=0, \tag{3}$$

$$\frac{\partial}{\partial x}\left[\rho u\left(e+\frac{1}{2}(u^2+v^2)+\frac{P}{\rho}\right)\right]+\frac{\partial}{\partial y}\left[\rho v\left(e+\frac{1}{2}(u^2+v^2)+\frac{P}{\rho}\right)\right]=0, \tag{4}$$

$$\frac{\partial}{\partial x}(\rho u\lambda_1)+\frac{\partial}{\partial y}(\rho v\lambda_1)=\kappa\rho(1-\lambda_1)\exp\left(\frac{-\epsilon\Theta_1}{T}\right), \tag{5}$$

$$\frac{\partial}{\partial x}(\rho u\lambda_2)+\frac{\partial}{\partial y}(\rho v\lambda_2)=\rho(\lambda_1-\lambda_2)\exp\left(\frac{-\epsilon\Theta_2}{T}\right), \tag{6}$$

$$e=1/(\gamma-1)(P/\rho)-\epsilon(\lambda_1 q_1+\lambda_2 q_2), \tag{7}$$

$$P=\rho T. \tag{8}$$

The variables contained in Eqs. (1)–(8) are the density ρ, Cartesian velocity components u and v, pressure P, temperature T, internal energy e, and reaction progress variables λ_1 and λ_2. The Cartesian position coordinates are x and y. The parameter ϵ is defined as the reciprocal of the square of the free-stream Mach number ($\epsilon=1/M_0^2$). Other dimensionless parameters are the ratio of specific heats γ, a kinetic constant κ, the heats of reaction q_1 and q_2, and the activation energies Θ_1 and Θ_2.

Equations (1)–(4) represent the conservation of mass, x momentum, y momentum, and energy, respectively. Equations (5)–(6) are species evolution equations that incorporate an Arrhenius depletion model. A two-step reaction mechanism is employed, $A\rightarrow B\rightarrow C$, in which the first reaction is exothermic and the second reaction is endothermic. The subscripts "1" and "2" correspond to the first and second reaction, respectively. Here, λ_1 and λ_2 both range from zero before reaction to unity at complete reaction. Species mass fractions Y_i are related to λ_1 and λ_2 by the formulas $Y_A=1-\lambda_1$, $Y_B=\lambda_1-\lambda_2$, and $Y_C=\lambda_2$. Equations (7)–(8) are the caloric and thermal state equations. Equation (7) suggests the adoptation of the dimensionless net chemical heat release Q as a function of λ_1 and λ_2: $Q(\lambda_1,\lambda_2)=\lambda_1 q_1+\lambda_2 q_2$.

Initial preshock conditions are specified as

$$\rho=1, \quad u=\sqrt{\gamma}\sin\beta, \quad v=\sqrt{\gamma}\cos\beta,$$
$$P=\epsilon, \quad \lambda_1=0, \quad \lambda_2=0. \tag{9}$$

Equations (1)–(8) have been scaled such that, in the hypersonic limit ($\epsilon\rightarrow 0$), the postshock pressure, density, and velocities are all $O(1)$ quantities and the effects of reaction are restricted to $O(\epsilon)$ or less. There are two length scales: the reaction zone lengths of the exothermic and endothermic reactions. The reaction zone length associated with the endothermic reaction is chosen as the reference length scale. In terms of dimensional variables (indicated by the notation "$\sim$") and dimensional preshock ambient conditions (indicated by the subscript "0"), the dimensionless variables are defined by

$$\rho=\frac{\tilde{\rho}}{\tilde{\rho}_0}, \quad P=\frac{\tilde{P}}{M_0^2\tilde{P}_0}, \quad u=\frac{\tilde{u}}{M_0\sqrt{\tilde{P}_0/\tilde{\rho}_0}},$$
$$v=\frac{\tilde{v}}{M_0\sqrt{\tilde{P}_0/\tilde{\rho}_0}}, \quad x=\frac{\tilde{k}_2\tilde{x}}{M_0\sqrt{\tilde{P}_0/\tilde{\rho}_0}}, \quad y=\frac{\tilde{k}_2\tilde{y}}{M_0\sqrt{\tilde{P}_0/\tilde{\rho}_0}}. \tag{10}$$

Remaining dimensionless parameters are defined by the following relations:

$$q_1=\frac{\tilde{\rho}_0\tilde{q}_1}{\tilde{P}_0}, \quad q_2=\frac{\tilde{\rho}_0\tilde{q}_2}{\tilde{P}_0}, \quad \kappa=\frac{\tilde{k}_1}{\tilde{k}_2},$$
$$\Theta_1=\frac{\tilde{\rho}_0\tilde{E}_1}{\tilde{P}_0}, \quad \Theta_2=\frac{\tilde{\rho}_0\tilde{E}_2}{\tilde{P}_0}. \tag{11}$$

Here, $\tilde{E}_1$ and $\tilde{E}_2$ are the activation energies, and $\tilde{k}_1$ and $\tilde{k}_2$ are the kinetic rate constants.

III. PRELIMINARY ANALYSIS

Equations (1)–(6) are simplified by assuming there are no changes in the direction tangent to the shock; hence, $\partial/\partial y=0$. Using the subsequent result that ρu is invariant and eliminating e and T by use of Eqs. (7) and (8), the system reduces to the following set of ordinary differential equations:

$$\frac{d}{dx}(\rho u)=0, \tag{12}$$

$$\frac{d}{dx}(\rho u^2+P)=0, \tag{13}$$

$$\frac{dv}{dx}=0, \tag{14}$$

$$\frac{d}{dx}\left[\left(\frac{1}{\gamma-1}\frac{P}{\rho}-\epsilon Q(\lambda_1,\lambda_2)\right)+\frac{1}{2}(u^2+v^2)+\frac{P}{\rho}\right]=0, \tag{15}$$

$$\frac{d\lambda_1}{dx}=\kappa\frac{1-\lambda_1}{u}\exp\left(\frac{-\epsilon\Theta_1\rho}{P}\right), \tag{16}$$

$$\frac{d\lambda_2}{dx}=\frac{\lambda_1-\lambda_2}{u}\exp\left(\frac{-\epsilon\Theta_2\rho}{P}\right). \tag{17}$$

Consequences of these assumptions are that u depends only on x, and v is a constant through both the shock and reaction zone; hence, the entire flow field is irrotational.

Using the initial conditions (9), Eqs. (12)–(15) can be integrated to yield algebraic RH equations that are valid through both the shock and reaction zone:

$$\rho u=\sqrt{\gamma}\sin\beta, \tag{18}$$

$$\rho u^2+P=\gamma\sin^2\beta+\epsilon, \tag{19}$$

$$v=\sqrt{\gamma}\cos\beta, \tag{20}$$

$$\left(\frac{1}{\gamma-1}\frac{P}{\rho}-\epsilon Q(\lambda_1,\lambda_2)\right)+\frac{1}{2}(u^2+\gamma\cos^2\beta)+\frac{P}{\rho}$$
$$=\frac{1}{\gamma-1}\epsilon+\frac{\gamma}{2}+\epsilon. \tag{21}$$

When $Q(\lambda_1,\lambda_2)=0$, Eqs. (18)–(21) reduce to standard inert oblique shock equations. This is expected as it can be formally shown from Eqs. (1)–(8) that through an inert shock, modeled as infinitely thin, reaction has no time to take place, and the jump in reaction progress is zero.

Equations (18), (19), and (21) can be solved for ρ, u, and P as functions of λ_1, λ_2. These relations are presented in a form equivalent to that of Gross:[4]

$$\rho(\lambda_1,\lambda_2)=\left(\frac{1+\gamma(1/\epsilon)\sin^2\beta\pm\sqrt{A(\lambda_1,\lambda_2)}}{(\gamma+1)(1/\epsilon)\sin^2\beta}\right)^{-1},$$

where

$$A(\lambda_1,\lambda_2)=\left[1+\gamma\left(\frac{1}{\epsilon}\right)\sin^2\beta\right]^2-(\gamma+1)\left(\frac{1}{\epsilon}\right)\sin^2\beta\left[2+2Q(\lambda_1,\lambda_2)\frac{(\gamma-1)}{\gamma}+(\gamma-1)\left(\frac{1}{\epsilon}\right)\sin^2\beta\right], \tag{22}$$

$$u(\lambda_1,\lambda_2)=\sqrt{\gamma}\sin\beta/\rho(\lambda_1,\lambda_2), \tag{23}$$

$$P(\lambda_1,\lambda_2)=\epsilon+\gamma\sin^2\beta[1-1/\rho(\lambda_1,\lambda_2)]. \tag{24}$$

For small Q, the "$-$" root of Eq. (22) is a perturbation of the shocked state, and the "$+$" root is a perturbation of the unshocked state. The two branches are thus called the shocked and unshocked branches, respectively.

With the pressure, density, and velocity fields parametrized by λ_1 and λ_2, Eqs. (16) and (17) can be expressed in the form

$$\frac{d\lambda_1}{dx}=f_1(\lambda_1,\lambda_2),\quad \lambda_1(0)=0, \tag{25}$$

$$\frac{d\lambda_2}{dx}=f_2(\lambda_1,\lambda_2),\quad \lambda_2(0)=0. \tag{26}$$

Equations (25) and (26) are integrated numerically to find λ_2 and λ_2 as functions of x; thus Q, and subsequently ρ, P, u, e, and T, can be calculated throughout the reaction zone.

IV. HYPERSONIC LIMIT

In the hypersonic limit ($\epsilon\to 0$), a closed form asymptotic solution can be obtained. In this limit, the chemical energy release only slightly disturbs the flow, which has a large kinetic energy. Equations (22)–(24) solved in this limit to $O(\epsilon)$ yield

$$\rho(\lambda_1,\lambda_2)=\frac{\gamma+1}{\gamma-1}-\epsilon\frac{(\gamma+1)^2}{(\gamma-1)\gamma\sin^2\beta}\left(Q(\lambda_1,\lambda_2)+\frac{2\gamma}{\gamma^2-1}\right), \tag{27}$$

$$u(\lambda_1,\lambda_2)=\frac{\sqrt{\gamma}(\gamma-1)\sin\beta}{(\gamma+1)}+\epsilon\frac{(\gamma-1)}{\sqrt{\gamma}\sin\beta}\left(Q(\lambda_1,\lambda_2)+\frac{2\gamma}{\gamma^2-1}\right), \tag{28}$$

$$P(\lambda_1,\lambda_2)=\frac{2\gamma\sin^2\beta}{\gamma+1}-\epsilon(\gamma-1)\left(Q(\lambda_1,\lambda_2)+\frac{1}{\gamma+1}\right). \tag{29}$$

In Eqs. (16) and (17) at $O(1)$, the argument of the exponential function is zero, and the velocity u has its constant $O(1)$ postshock value. Thus these equations may be integrated to give the $O(1)$ reaction zone structure explicitly:

$$\lambda_1=1-\exp\left(-\frac{\kappa(\gamma+1)x}{\sqrt{\gamma(\gamma-1)}\sin\beta}\right), \tag{30}$$

$$\lambda_2=1-\left(1+\frac{(\gamma+1)x}{\sqrt{\gamma(\gamma-1)}\sin\beta}\right)\times\exp\left(-\frac{(\gamma+1)x}{\sqrt{\gamma(\gamma-1)}\sin\beta}\right)\quad(\kappa=1), \tag{31}$$

$$\lambda_2=1-\left(\frac{\kappa}{\kappa-1}\right)\exp\left(-\frac{(\gamma+1)x}{\sqrt{\gamma(\gamma-1)}\sin\beta}\right)+\left(\frac{1}{\kappa-1}\right)\times\exp\left(-\frac{\kappa(\gamma+1)x}{\sqrt{\gamma(\gamma-1)}\sin\beta}\right)\quad(\kappa\neq 1). \tag{32}$$

When the reaction progress field (30)–(32) is substituted into Eqs. (27)–(29), one obtains the pressure, velocity, and density fields to $O(\epsilon)$.

The value of the asymptotic solution lies in its use as an independent check of the numerical solution of Eqs. (22)–(26). Subsequent results will show that the asymptotic and numerical solutions show the same trends. Furthermore, it can be easily verified that, when a sufficiently small step size is chosen for the numerical integration, that in the limit as $\epsilon\to 0$, the difference between the asymptotic and numerical solution approaches zero at $O(\epsilon)$ and is bounded at $O(\epsilon^2)$ as expected.

V. RESULTS

In this section, we give results, not restricted to the hypersonic limit, for P, λ_1 phase portraits for several values of β and their relation to oblique detonation polars, streamlines, and characteristics, an example of oblique detonation structure for each solution class: I, strong; II, weak overdriven; and III, weak underdriven, and an illustration of the behavior of the weak underdriven solution as q_2 is varied with the net complete reaction heat release $Q(1,1)$ held constant.

In all calculations, except the last, which considers variable q_2, we take $\epsilon=1/100$ (so that the incoming Mach number is 10), $\gamma=7/5$, $\kappa=1$, $\Theta_1=\Theta_2=0$, $q_1=100$, and $q_2=-75$. For case I, we take a representative angle, $\beta=80°$. For case II, we take a representative angle, $\beta=60°$. For case III, an eigenvalue wave angle is found to be $\beta=\tilde{\beta}=52.77°$. For these three cases, the respective labels I, II, and III are adopted. Phase portraits are also presented at the detachment wave angle for this system, $\beta=\beta_{\text{detach}}=65.65°$, at the subsonic to supersonic transition wave angle, $\beta=\beta_{\text{SS}}=65.53°$, for a representative shockless structure with turning angle $\beta=60°$, for a representative structure for which there is no trajectory to complete reaction, $\beta=50°$, and for the CJ wave angle for which there is also no trajectory to complete reaction, $\beta=\beta_{\text{CJ}}=37.02°$.

A. Phase space portraits and detonation polars

Equations (25) and (26) were integrated numerically using a Runge–Kutta technique. Results are summarized in the P, λ_1 phase plane shown in Fig. 3. The variables ρ,

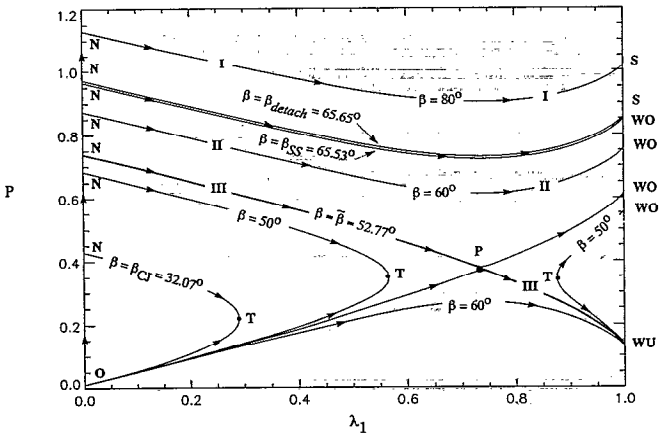

FIG. 3. P_1, λ_1 phase plane.

P, and u for structures with a lead shock are calculated using the shocked branch of Eq. (22). The flow is shocked from the inert state at O to the Neumann point N. For strong solutions such as case I, where $\beta_{\text{detach}} < \beta \leqslant 90°$, as the reaction progresses, the pressure decreases from its value at N to a pressure minimum and then increases to its final value at the strong point S. The phase space trajectories are topologically equivalent for weak overdriven solutions such as case II, for both $\beta_{\text{SS}} < \beta \leqslant \beta_{\text{detach}}$ and $\tilde{\beta} < \beta \leqslant \beta_{\text{SS}}$. In such cases, the trajectory begins at O, is shocked to N, and terminates at WO. There is also nothing topological to distinguish the trajectories at either $\beta = \beta_{\text{detach}}$ or $\beta = \beta_{\text{SS}}$, which are also plotted in Fig. 3. As the difference between β_{detach} and β_{SS} is small, the difference in the two trajectories has been slightly exaggerated so they can be distinguished on this scale.

The case I trajectory, O–N–S, and case II trajectory, O–N–WO, are also plotted in β, θ space on the polars of Fig. 4. On each trajectory, the fluid reacts with the exothermic reaction dominant until the heat release reaches a local maximum, $Q_{\max}$ at which point the endothermic reaction dominates until complete reaction when $Q=25$. In these and all cases studied, $Q_{\max}$ was nearly constant at 44.8.

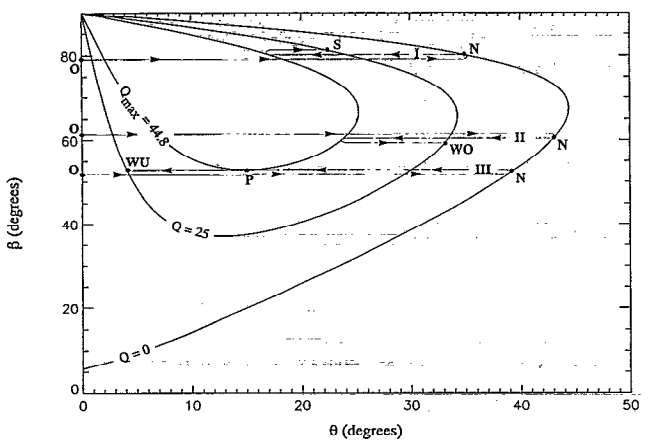

FIG. 4. Inert ($Q=0$), intermediate ($Q=44.8$), and complete reaction ($Q=25$) polars along with strong (case I), weak overdriven (case II), and weak underdriven (case III) phase trajectories.

The behavior of the P, λ_1 trajectories can be predicted by using Eqs. (12)–(17) to explicitly solve for the pressure derivative:

$$\frac{dP}{dx} = \epsilon \frac{(\gamma-1)\rho u^2 [q_1(d\lambda_1/dx) + q_2(d\lambda_2/dx)]}{u^2 - \gamma(P/\rho)}. \quad (33)$$

Using Eqs. (22)–(24) to evaluate ρ, u, and P downstream of the shock along with Eqs. (16) and (17) to evaluate reaction progress derivatives, it is easily shown that just past the shock, $dP/dx < 0$. It is also seen that $u > 0$; thus, from Eq. (16), it is deduced that λ_1 is a monotonically increasing function of x. Thus pressure variations with x and λ_1 are qualitatively similar. The predicted pressure minimum is a consequence of the quantity $q_1(d\lambda_1/dx) + q_2(d\lambda_2/dx) = dQ/dx$ reaching zero at an interior point of the reaction zone. As the reaction progress derivatives for the irreversible reaction scheme are always positive; this zero can only be reached if one reaction is exothermic and the other endothermic.

As β is reduced from 90°, it is possible to predict a continuum of strong solutions until $\beta = \beta_{\text{detach}}$ and a continuum of weak overdriven solutions from $\beta = \beta_{\text{detach}}$ until a certain eigenvalue wave angle $\beta = \tilde{\beta}$ is reached. At $\beta = \tilde{\beta}$, the solution trajectories reach a saddle critical point, labeled P for pathological, in P, λ_1 phase space. At P, dQ/dx and $u^2 - \gamma P/\rho$ are simultaneously zero; i.e., the heat release rate approaches zero as the local Mach number approaches unity. It is also seen that the quantity A in Eq. (22) is simultaneously zero. Thus integration can be continued on either the shocked or unshocked branch of Eq. (22). Integration along the shocked branch carries the trajectory to a final weak overdriven state WO, while if the unshocked branch is selected, the solution proceeds to completion to the weak underdriven point WU. The case III trajectory, O–N–P–WU, is plotted in Figs. 3 and 4.

For solutions with $\beta > \tilde{\beta}$, which remain on the unshocked branch, a complementary family of solutions exists. One such trajectory from O to WU is shown in Fig. 3. The physical justification for the unshocked solution is not clear-cut as there is no distinct initiation mechanism and the equations are subject to the cold boundary difficulty.

For $\beta < \tilde{\beta}$, there is no trajectory to complete reaction. In P, λ_1 phase space, one family of such trajectories is in the neighborhood near $\lambda_1 = 0$. These trajectories originate at N or O and progress to a termination point T where the flow reaches a local sonic state at a point where the heat release rate dQ/dx is nonzero. A complementary family of trajectories exists in the neighborhood of $\lambda_1 = 1$. These originate at the complementary T and terminate at either WO or WU. A representative trajectory for $\beta = 50°$ is plotted in Fig. 3. For the parameters of these example problems, $\beta_{\text{CJ}} = 37.02° < \tilde{\beta}$; consequently, there is no complete reaction CJ trajectory. The trajectory for the CJ angle is also plotted in Fig. 3.

B. Streamlines and characteristics

Standard expressions for streamlines and characteristics for two-dimensional steady compressible flow, such as those given by Shapiro,[10] also apply to this reactive flow field. The family of streamlines $y_s(x)$ and characteristics $y_\pm(x)$ are generated from the known field variables by the following expressions:

$$y_s(x)=\sqrt{\gamma}\cos\beta\int_{x_0}^{x}\frac{d\breve{x}}{u(\breve{x})}, \tag{34}$$

$$y_\pm(x)=\int_{x_0}^{x}\frac{\sqrt{\gamma}\cos\beta u(\breve{x})/a^2(\breve{x})\pm\sqrt{M^2(\breve{x})-1}}{M_x^2(\breve{x})-1}d\breve{x},$$

with

$$a^2(x)=\gamma\frac{P(x)}{\rho(x)},\quad M_x^2(x)=\frac{u^2(x)}{a^2(x)},$$
$$M^2(x)=\frac{u^2(x)+\gamma\cos^2\beta}{a^2(x)}. \tag{35}$$

Here, $\breve{x}$ is a dummy variable; x_0 gives the initial x position of a particular streamline or characteristic; and a is the local sound speed. The streamline for $x_0=0$ is taken to be coincident with a solid curved wedge that supports the oblique detonation. The characteristics are real when $M>1$; the characteristics are parallel to the shock when $M_x=1$.

In the following examples, cases I, II, and III, we will plot the streamlines and characteristics in the $(\hat{x},\hat{y})$ orthogonal coordinate system, which is defined to be aligned with the incoming flow. The appropriate transformations for this system are $\hat{x}=x\sin\beta+y\cos\beta$, and $\hat{y}=-x\cos\beta+y\sin\beta$. The trajectories for cases I, II, and III have been plotted in Figs. 3 and 4.

C. Strong, case I

We give an example of a strong oblique detonation in which $\beta=80°$. For this case, $M<1$ and $M_x<1$ throughout the reaction zone. Reaction zone profiles for reaction progress, λ_1, λ_2, and pressure P predicted by both the numerical and asymptotic methods are shown in Figs. 5(a) and 5(b). The asymptotic and numerical predictions follow the same trends. Since $M<1$, the steady flow field is elliptic, there are no real characteristics, and disturbances at any location are propagated to the entire flow field. The domain of dependency for any point on the shock is the entire region between the shock and the wedge. The streamlines for the strong solution are shown in Fig. 5(c).

D. Weak overdriven, case II

We next consider a weak overdriven oblique detonation in which $\beta=60°$. In this case, $M>1$ while $M_x<1$ throughout the reaction zone. Figures 6(a)–6(c) show the reaction zone profiles for λ_1, λ_2, and P, streamlines and characteristics, respectively. The numerical and asymptotic predictions are in qualitative agreement and also resemble those of the strong oblique detonation case. All characteristics of the "+" family that originate on the wedge surface intersect the shock at a downstream location. The domain of dependency for a given point on the shock is limited to points upstream of the "+" characteristic that intersect this point.

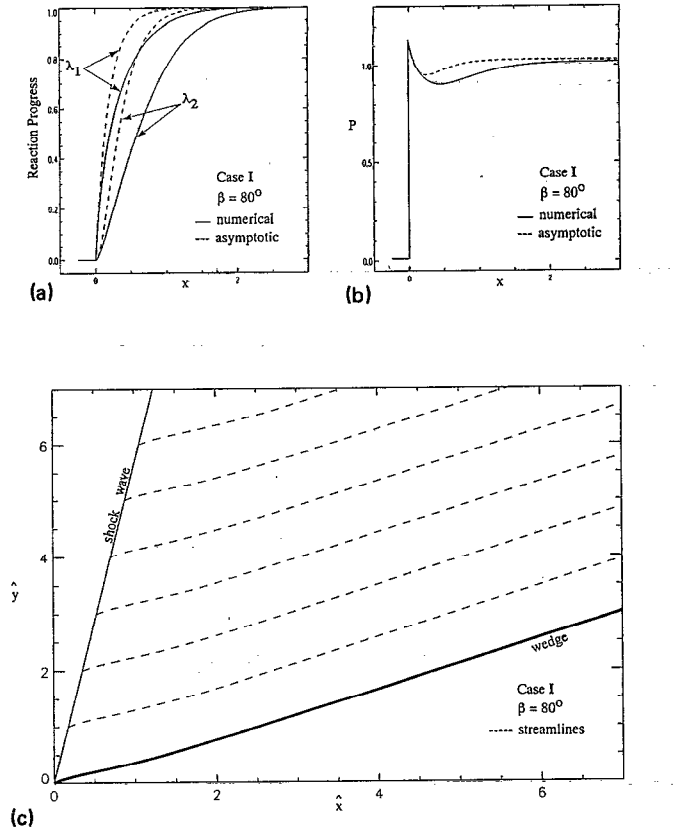

FIG. 5. (a) Predictions of the reaction progress variables for a strong oblique detonation. (b) Predictions of pressure for a strong oblique detonation. (c) Streamlines for a strong oblique detonation.

E. Weak underdriven, case III

We finally consider a weak underdriven (eigenvalue) oblique detonation, which for the parameters of this study, occurs at $\beta=\tilde{\beta}=52.77°$. In this case, $M>1$, while M_x is subsonic near the shock and supersonic downstream of the shock. Figures 7(a)–7(c) show the reaction zone profiles for λ_1, λ_2, and P, streamlines and characteristics, respectively. For small x the structure is similar to the weak overdriven structure. Upon reaching the pathological point P, the structure changes dramatically. The pressure P does not reach a local minimum but monotonically decreases to its value at complete reaction. The streamlines behave similarly to those of the previous two cases.

The characteristics behave much differently. Characteristics of the "+" family that originate at the wedge surface near the wedge tip intersect the shock. At a critical location on the wedge surface, which occurs when $M_x=1$, the "+" characteristic is parallel to the lead shock. Characteristics that originate on the wedge surface past this point do not intersect the lead shock. Thus the domain of dependency for any point on the shock is limited to a finite

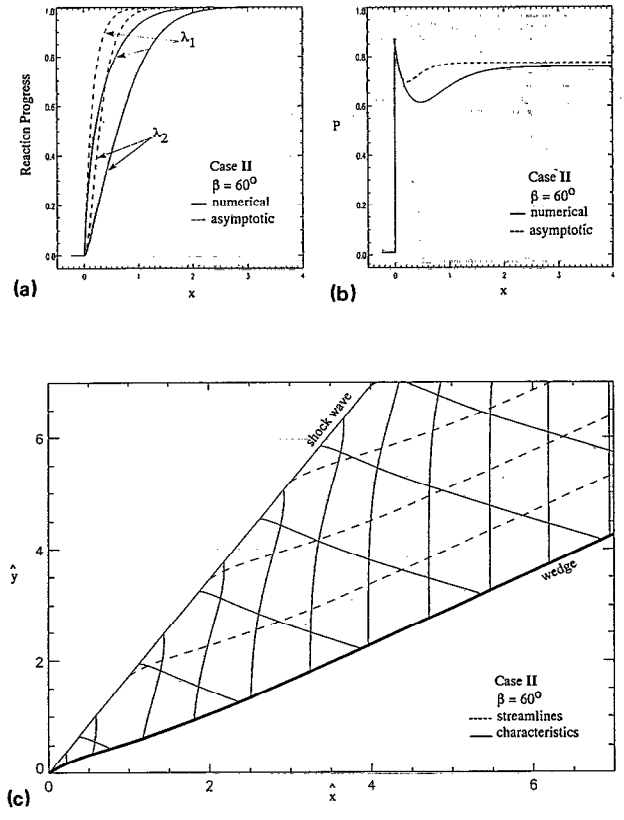

FIG. 6. (a) Predictions of the reaction progress variables for a weak overdriven oblique detonation. (b) Predictions of pressure for a weak overdriven oblique detonation. (c) Streamlines and characteristics for a weak overdriven oblique detonation.

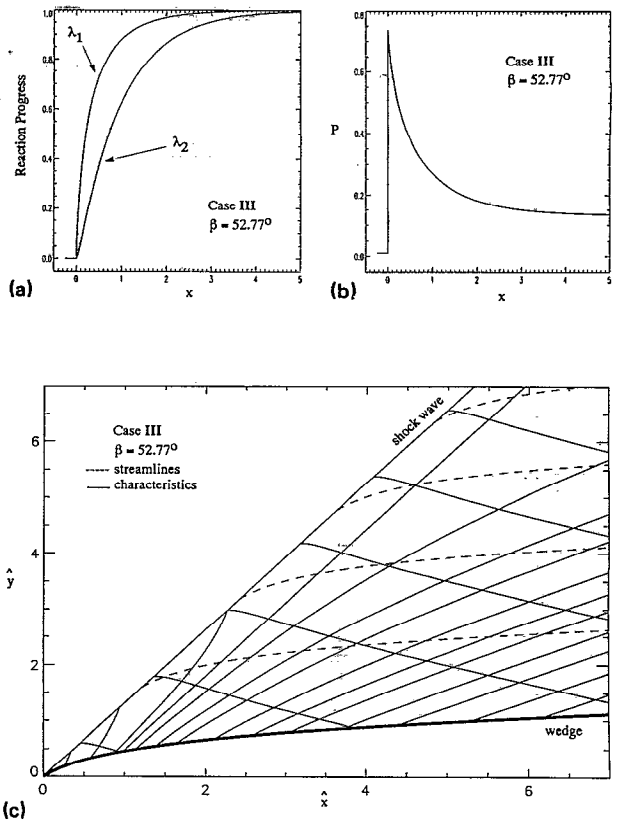

FIG. 7. (a) Numerical prediction of the reaction progress variables for a weak underdriven oblique detonation. (b) Numerical prediction of pressure for a weak underdriven oblique detonation. (c) Streamlines and characteristics for a weak underdriven oblique detonation.

width zone near the shock and is upstream of a given "+" characteristic. Points in the domain downstream of the sonic characteristic do not influence the upstream flow; consequently, there is a wider variety of solutions possible, not shown here, that are consistent with a flow characterized by a straight shock.

F. Effect of variable relative endothermicity

Figure 8 demonstrates the effect of variable relative endothermicity on the eigenvalue wave angle $\tilde{\beta}$. To obtain this plot, we simultaneously adjust the value of both q_1 and q_2 such that the global heat release at complete reaction is maintained at $Q(1,1)=25$. For $-75 \leqslant q_2 < 0$ (and, simultaneously, $100 \geqslant q_1 > 25$) as q_2 is increased toward 0, $\tilde{\beta}$ decreases. When $q_2=0$, the point P becomes coincident with the CJ point, and $\tilde{\beta}=\beta_{CJ}=37.02°$. For $0 < q_2 \leqslant 25, 25 > q_1 \geqslant 0$ both reactions are exothermic, there is no eigenvalue solution, and the CJ solution is the limiting solution. Solutions outside this range were not studied. Thus, in this range, the model only predicts strong, weak overdriven, and CJ solutions. This result is consistent with the results obtained in Ref. 8 where $q_2=0$.

VI. FINAL REMARKS

This study has demonstrated the critical role that the kinetic scheme can play in determining admissible oblique detonation structures. For the kinetic scheme of this study, the CJ state has relatively little significance. It provides only an overly conservative lower bound for the wave angle, with the true boundary more restrictive. One can in-

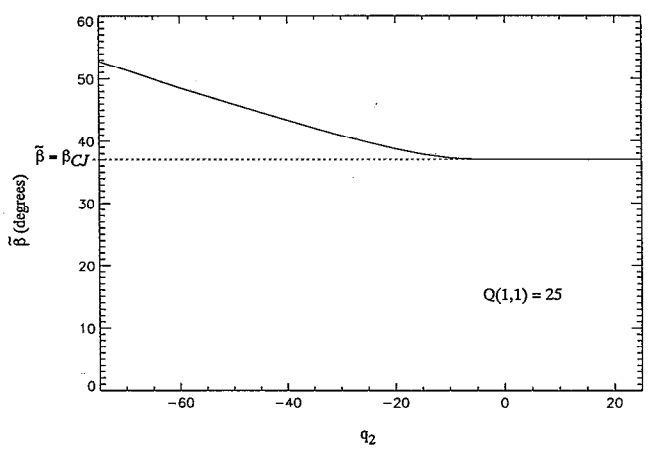

FIG. 8. Eigenvalue wave angle $\tilde{\beta}$ as a function of heat released in second reaction q_2 with global heat release $Q(1,1)$ held constant.

duce for reaction schemes with more complex kinetics that the necessary conditions for admissible solutions become correspondingly more complex.

Though the flow physics are different, these oblique detonation flows have a remarkably similar mathematical structure to such classical flows[10] as (1) one-dimensional Rayleigh flow, or (2) one-dimensional inert flow with area change. For instance, flow at the pathological point P is analogous to a one-dimensional inert flow simultaneously reaching an area minimum and a local sonic state. The one-dimensional inert flow is able to relax to a variety of downstream boundary conditions when one allows either a normal shock to stand in the duct or downstream rarefactions. Consequently, we hypothesize that there is a wider range of oblique detonation solutions available when one allows for either a more complex structure with additional shocks or rarefactions.

The stability of these waves is open to question. Powers and Stewart[8] have given an example of the structural stability of irrotational weak overdriven oblique detonations. They showed straightening the curved wedge only changes the flow field by introducing a small amount of vorticity near the wedge surface and that far from the wedge, the solution remains the same, with a straight shock and curved streamlines. Since the weak overdriven solutions of this study are perturbations of those of Ref. 8, these too may be structurally stable to changes in the wedge shape. The weak underdriven case presented here is structurally unstable. Any parametric change would result in no steady solution with a single attached shock. The weak underdriven solution may still be of value, however, if, for instance, (1) the solution is a degenerate case of a solution with a more complicated shock or rarefaction structure, or (2) effects not modeled here, such as diffusive transport effects, have the consequence of being stabilizing influences. Grismer and Powers[11] have shown that the oblique detonations of Ref. 8 are numerically stable for one particular numerical method. Again, since the weak overdriven solutions of this study are perturbations of those studied in Ref. 11, they should also be numerically stable. Recent studies by Buckmaster,[12] Jackson *et al.*,[13] and Lasseigne *et al.*[14] have considered hydrodynamic stability and related questions for weak overdriven oblique detonations using one-step kinetics.

ACKNOWLEDGMENTS

This study was sponsored by the 1991 NASA-ASEE Summer Faculty Fellowship Program and the University of Notre Dame. A portion of this work was conducted during the authors' residence at the NASA Lewis Research Center.

This paper was originally presented at the 30th Aerospace Sciences Meeting and Exhibit 6–9 January, Reno, Nevada.

[1] R. Siestrunck, J. Fabri, and E. Le Grivès, "Some properties of stationary detonation waves," in *Proceedings of the Fourth Symposium (International) on Combustion* (Williams and Wilkins, Baltimore, MD, 1953), pp. 498–501.

[2] E. Larisch, "Interactions of detonation waves," J. Fluid Mech. **6**, 392 (1959).

[3] R. A. Gross and W. Chinitz, "A study of supersonic combustion," J. Aerosp. Sci. **27**, 517 (1960).

[4] R. A. Gross, "Oblique detonation waves," AIAA J. **1**, 1225 (1963).

[5] A. K. Oppenheim, J. J. Smolen, and L. J. Zajac, "Vector polar method for the analysis of wave intersections," Combust. Flame **12**, 63 (1968).

[6] G. G. Chernyi, "Supersonic flow past bodies with formation of detonation and combustion fronts," *Problems of Hydrodynamics and Continuum Mechanics*, English ed. (SIAM, Philadelphia, PA, 1969), pp. 145–169.

[7] D. T. Pratt, J. W. Humphrey, and D. E. Glenn, "Morphology of a standing oblique detonation wave," J. Propulsion Power **7**, 837 (1991).

[8] J. M. Powers and D. S. Stewart, "Approximate solutions for oblique detonations in the hypersonic limit," AIAA J. **30**, 726 (1992).

[9] W. Fickett and W. C. Davis, *Detonation* (University of California Press, Berkeley, 1979).

[10] A. H. Shapiro, *The Dynamics and Thermodynamics of Compressible Fluid Flow* (Wiley, New York, 1953), Vol. I.

[11] M. J. Grismer and J. M. Powers, "Comparison of numerical oblique detonation solutions with an asymptotic benchmark," to appear in AIAA J.

[12] J. Buckmaster, "The structural stability of oblique detonation waves," Combust. Sci. Technol. **72**, 283 (1990).

[13] T. L. Jackson, A. K. Kapila, and M. Y. Hussaini, "Convection of a pattern of vorticity through a reacting shock wave," Phys. Fluids A **2**, 1260 (1990).

[14] D. G. Lasseigne, T. L. Jackson, and M. Y. Hussaini, "Nonlinear interaction of a detonation/vorticity wave," Phys. Fluids A **3**, 1972 (1991).